Modeling of stress-strain dependences for Berea sandstone under quasistatic loading

Vyacheslav O. Vakhnenko,[1,*] Oleksiy O. Vakhnenko,[2,†] James A. TenCate,[3,‡] and Thomas J. Shankland[3,§]
[1]*Institute of Geophysics, Kyïv 01054, Ukraine*
[2]*Bogolyubov Institute for Theoretical Physics, Kyïv 03143, Ukraine*
[3]*Los Alamos National Laboratory, Los Alamos, New Mexico 87545, USA*
(Received 26 February 2007; published 9 November 2007)

In this work, a phenomenological model to describe the complex stress-strain properties of a sandstone sample under slow loading is presented. We consider a combination of three methods to treat the elastic and nonlinear behavior observed in stress cycling experiments. The mechanisms to treat interior equilibration processes in sandstone are termed the standard solid relaxation mechanism, the sticky-spring mechanism, and the permanent plastic deformation mechanism. With a small number of parameters, the overall model displays both qualitatively and quantitatively the principal experimental observations of the stress-strain trajectories for Berea sandstone, in particular, the details of end-point memory under quasistatic loading.

DOI: 10.1103/PhysRevB.76.184108 PACS number(s): 62.20.Fe, 81.40.Jj, 62.40.+i, 91.60.Fe

I. INTRODUCTION

The typical stress-strain dependences for rocks under quasistatic loading measurements point out their essentially nonlinear behavior. Results by Adams and Coker,[1] Boitnott,[2] Hilbert *et al.*,[3] and Darling *et al.*[4] on repeatable hysteretic loops in stress-strain curves are well known and can be regarded as the classical experiments. Dealing only with macroparameters such as stress and strain while the processes on a microlevel still remain unknown makes it very difficult to create a model that adequately describes these properties. Recent experiments[4] showed that the most remarkable stress-strain properties of rocks are determined by a small volume of material at grain contacts. However, it is unclear how interior equilibration processes in rocks under quasistatic loading can be studied in detail. In the literature, there are a number of models that qualitatively describe the relationships between macroparameters such stress and strain. First of all, there are two models, the Hertz-Mindlin model[5] and the Preisach-Mayergoyz model.[6,7] However, with these approaches, there is some difficulty in assigning a set of model hysteretic elements to real physical processes. While these approaches can duplicate experimental observations, the incorrectly formulated connection between the distribution of auxiliary elements and maximum stress levels leads to their limited predictive power.

In this paper, we suggest three appropriately formalizing mechanisms that appear to actually occur in rocks under quasistatic loading: (i) a "standard solid relaxation" mechanism, (ii) a "sticky-spring" mechanism, and (iii) a "permanent plastic deformation" mechanism. A suitable combination of these mechanisms enables us to derive some general stress-strain relations, although without a detailed description of interior equilibration processes. As a result, we can obtain a phenomenological model that allows us to simulate qualitative and quantitative stress-strain characteristics and to reproduce the distinctive features typical of the basic experimental observations by Boitnott,[2] Hilbert *et al.*,[3] and Darling *et al.*[4] for Berea sandstone.

II. ANALYSIS OF EXPERIMENTAL DATA

In order to facilitate analysis of three groups of fundamental experimental data for Berea sandstone by Boitnott (Fig. 1 in Ref. 7), Hilbert *et al.* (Fig. 2 in Ref. 7), and Darling *et al.* (Fig. 1 in Ref. 4), we place them in a common format. Because in different experiments the origins of strain coordinates were introduced in different ways, it is an advantage to combine all experimental stress-strain curves in a single picture. We proceed from the assumption that for all three experimental curves, the points relating to maximum stress should be placed somewhere on the longest of the available unconditioned curves, i.e., on the bottom curve of Fig. 1(c), while the origin for the common strain coordinate should be chosen from Fig. 1(a), where the starting point of the unconditioned (bottom) curve is documented. In this terminology, "unconditioned" refers to an initial curve that starts at zero stress on a sample that has been undisturbed for a long period (of the order of many hours or a day) as is the case in Fig. 1(a). In contrast, the curves of Fig. 1(b) are "conditioned," that is, have undergone multiple stress cycles. In this case, the starting point is not shown and, except for the final, highest point, the unconditioned curve is absent. The original experimental figures have different scales, and in Fig. 1, we have placed the experimental curves (omitting the scale numbers for clarity) into common coordinates. In this procedure, Fig. 1(a) preserves its coordinates, while Figs. 1(b) and 1(c) are shifted to include zero strain positions; the strain shift for Fig. 1(a) is 0, for Fig. 1(b) is 0.000 42, and for Fig. 1(c) is 0.000 97.

It is pertinent to note that this approach for introducing common coordinates is not ideal inasmuch as it essentially treats the actual position of the initial (unconditioned) curve as independent of the rate of increase of the applied stress, which, in general, is not the case. However, experimentally, such a rate dependence is mainly detectable at high stresses and, to first (but rather good) approximation, can be neglected without practical consequences within the common frame of reference.

The first effect that arises within a detailed analysis of given experimental data as in Fig. 1 is the manifestation of some internal relaxation process that appears as a characteristic looplike retardation in strain response upon external loading and unloading stresses. Indeed, the experiment involving transient stress steps[8,9] clearly displays this effect. Relaxation component in the strain response can also be ob-

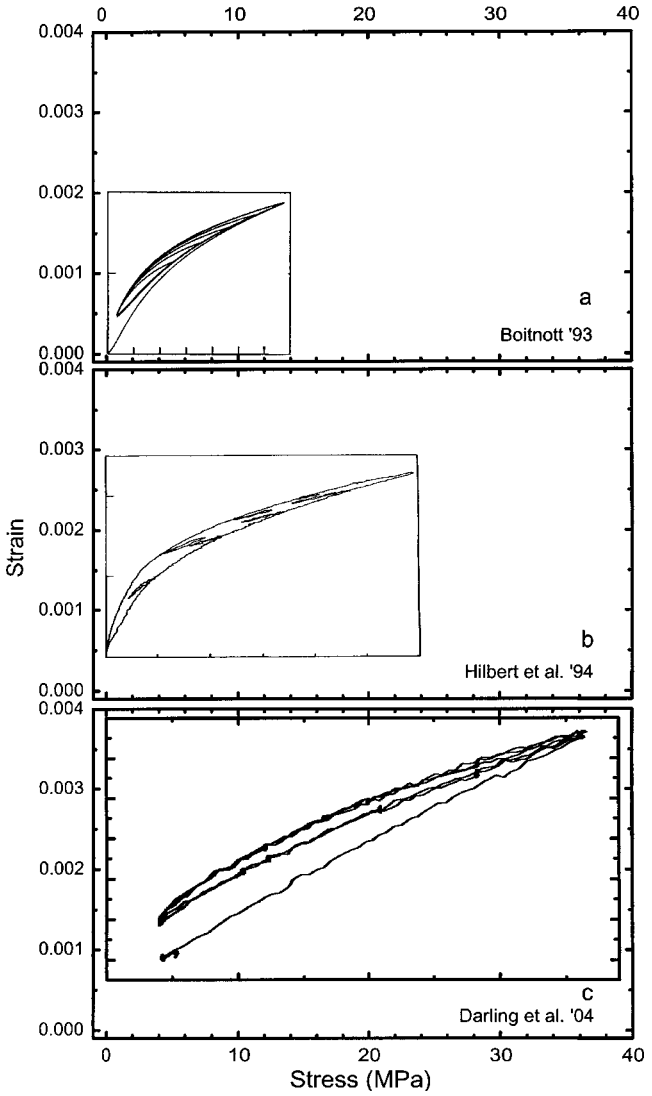

FIG. 1. Experimental results for Berea sandstone: (a) Boitnott (Ref. 2), (b) Hilbert *et al.* (Ref. 3), (c) and Darling *et al.* (Ref. 4). Stress-strain trajectories with their original coordinate meshes are placed within common coordinates. The systematic strain shifts caused by the apparatus adjustments are 0 for the data of Boitnott, 0.000 42 for the data of Hilbert *et al.*, and 0.000 97 for the data of Darling *et al.*

served in other stress-strain dependences for various sandstones,[4] especially for Meule sandstone. In particular, we see that after the moment when stress becomes constant, strain still changes for some time. Recently, several theoretical approaches have been developed to model time dependence in sandstone behavior near the high frequency vibrational resonance[10–13] as well as dispersion and absorption of sound in microinhomogeneous materials;[14] nevertheless, none of them seems to apply to the present case of comparatively slow loading. Hence, we will describe the relaxation features of sandstones in alternative terms of a phenomenological standard solid relaxation mechanism arising from a nonlinear generalization[15] of well-established relaxation modeling in the framework of a standard linear solid.[16]

Second, stress cycling gives rise to hysteresis loops in stress-strain curves. Observing the experimental dependences from Ref. 4 (particularly Fig. 1 in Ref. 4) reveals that opposite sides of each loop are not entirely stuck together even at infinitely slow loading, that is, the loops persist independent of loading time. Hence, there must be specific irreversible interior changes responsible for loop formation, i.e., ones that cannot be attributed simply to relaxation. We presume that some sort of friction has to be involved in any mechanism responsible for this effect. Therefore, we are forced to take into account a second mechanism, referred to here as a sticky-spring mechanism, for describing this aspect of sandstone stress-strain properties.

Finally, the whole conception would be incomplete without including a third mechanism called here permanent plastic deformation. This third mechanism is needed to explain the observation that unconditioned and conditioned experimental curves differ from each other due to a permanent deformation, that is, a strain offset.

The next section provides a comprehensive treatment of these three mechanisms in order to model the interior processes that arise in rock samples under quasistatic compression.

III. MODEL APPROACHES

This paper treats uniaxial compression of a rock sample restricted to quasistatic loading. As a consequence, the equation of motion for the bulk of the sample can be written using a single spatial coordinate

$$\rho\ddot{u} = \partial\sigma/\partial x \tag{1}$$

and can be simplified by putting the left-hand-side (inertial) term to zero. As usual, this approximation is valid when the wave propagation time $\tau_L = L/c$ (where L is the sample length and c is sound velocity) is sufficiently less than the loading time $\tau_\sigma = \sigma/\dot{\sigma}$, i.e., $\tau_L \ll \tau_\sigma$. Here, stress σ relates to strain $\varepsilon \equiv \partial u/\partial x$ through both elastic and anelastic mechanisms, which are obtained beforehand from analysis of experimental data. Moreover, in this (slow loading) approximation, the stress turns out to be uniform along a sample and is determined by the absolute value of external loading, which plays the role of an external governing parameter. For the latter reason, we assign both σ and ε to be positive quantities as they are usually regarded in quasistatic compression experiments.

The fact that for interpretation of quasistatic experiments it is sufficient to operate directly with the stress-strain relation provides a good basis for understanding the main mechanisms of anelasticity and elasticity, especially nonlinear ones, as well as to formalize and verify them. As mentioned previously, we consider separately three mechanisms to account for interior processes in a rock sample under quasistatic loading: (i) the standard solid relaxation mechanism, (ii) the sticky-spring mechanism, and (iii) the permanent plastic deformation mechanism.

A. Standard solid relaxation mechanism

The first part ε^r of the total strain ε to be considered is associated with a relaxation mechanism caused by an interior

equilibration process. We use the superscript index r to distinguish ε^r from other contributions to ε. According to the analysis of experimental curves in Sec. II, ε^r may depend on time not only implicitly through the governing stress σ but also explicitly through relaxation. Thus, in general, strain can have different values at the same stress. However, the main hypothesis, which will be confirmed *a posteriori*, consists in assuming that strain also responds to stress variation in time or, more precisely, to the time derivative $\dot{\sigma}$.

The most general linear theory taking into account all of the above-mentioned effects (i.e., explicit strain relaxation in time as well as implicit time dependence through both σ and $\dot{\sigma}$) is readily derived from the Zener phenomenological model of a standard linear solid,[16]

$$\tau\dot{\varepsilon}^r + \varepsilon^r = \frac{\sigma}{M_R} + \frac{\dot{\sigma}\tau}{M_U}. \tag{2}$$

The theory deals with three material parameters: a relaxation time τ and two elastic moduli, relaxed M_R and unrelaxed M_U. Considering the quasistatic loading, we restrict our description to the condition $\tau_L \ll \tau$. Its main result is that steady-state strain response (i.e., response at $t/\tau \gg 1$) to a periodically oscillating stress $\sigma=\sigma_a \cos(\omega t+\varphi)$ can exhibit two different regimes, namely, a relaxed $\varepsilon^r=\sigma/M_R$ at low frequencies $\omega\tau \ll 1$ and an unrelaxed $\varepsilon^r=\sigma/M_U$ at high frequencies $\omega\tau \gg 1$.

Unfortunately, another basic result,

$$\varepsilon^r = \frac{\sigma_0}{M_R}\frac{t}{t_0} - \sigma_0\frac{M_U - M_R}{M_U M_R}\frac{\tau}{t_0}, \tag{3}$$

describing the steady-state strain response (i.e., response at $t/\tau \gg 1$) to a stress growing linearly with time $\sigma=(\sigma_0/t_0)t$ is usually misinterpreted due to neglect of the small second term. Meanwhile, similar "small" terms can play crucial roles in a complete understanding of quasistatic loading experiments and should be accurately taken into account. It is remarkable that the steady-state strain response [Eq. (3)] reveals two contributions that are distinct in origin. The first term contains the elastic contribution σ/M_R usually measured under infinitesimally slow loading, whereas the second term yields the regular anelastic shift proportional to the difference M_U-M_R, to τ, and to the loading rate σ_0/t_0. In contrast, the instantaneous strain response (i.e., response at $t/\tau \ll 1$) on the same stress $\sigma=(\sigma_0/t_0)t$ exhibits only the elastic contribution σ/M_U and is characterized by the unrelaxed elastic modulus M_U:

$$\varepsilon^r = \frac{\sigma_0}{M_U}\frac{t}{t_0}. \tag{4}$$

As for a possible physical background for modeling the standard linear solid, researchers often appealed to a hidden interior relaxation process.[17,18] Its main distinguishing feature consists of allowing the equilibrium state to shift linearly subject to an external influence, in particular, subject to applied external pressure and its time derivative.[18]

In order to extend the basic ideas of a standard linear solid and its physical justification, a more general theory to describe the additional effects of nonlinear elasticity was developed several years ago.[15] The appropriate dynamic state equation becomes

$$\tau\frac{d}{dt}[\varepsilon^r - \varepsilon_f^r(\sigma)] + \varepsilon^r - \varepsilon_e^r(\sigma) = 0. \tag{5}$$

The suggested relation between strain ε^r, stress σ, and their time derivatives $\dot{\varepsilon}^r$ and $\dot{\sigma}$ is distinguished to include nonlinearities by means of two essentially nonlinear functions $\varepsilon_e^r(\sigma)$, and $\varepsilon_f^r(\sigma)$. These functions are responsible for a true thermodynamic equilibrium state at infinitely slow loading and for a frozen pseudoequilibrium state at infinitely fast loading, respectively. Both slow and fast terms are understood in relation to the typical time τ characterizing hidden internal relaxation processes. Formally speaking, the curve $\varepsilon_e^r=\varepsilon_e^r(\sigma)$ could be thought as the state equation in the limit of instantaneous relaxation $\tau \to 0$, whereas the curve $\varepsilon_f^r=\varepsilon_f^r(\sigma)$ is the state equation in the limit of no relaxation $\tau \to \infty$.

It is necessary to note that, just as for the linear theory, the interior equilibration processes need not be specified concretely in the derivation of Eq. (5), but the macroscopic characteristics $\varepsilon_e^r(\sigma)$, $\varepsilon_f^r(\sigma)$, and τ in this approach are chosen to be a satisfactory combination for the overall model description. Of course, the macroscopic parameters involved, as well as the particular forms of functional dependences $\varepsilon_e^r(\sigma)$ and $\varepsilon_f^r(\sigma)$ themselves, should be selected to match known experimental results.

We term the model incorporated in the dynamical state equation [Eq. (5)] as the standard solid relaxation mechanism in view of its generic property of interconnection of two different nonlinear elastic state equations mediated through the hidden interior relaxation processes, similar to the interconnection of two linear state equations in the theory of standard linear solid. In what follows, the equilibrium state function $\varepsilon_e^r(\sigma)$ is determined by the ordinary formula

$$\varepsilon_e^r(\sigma) = [E_e(\sigma)]^{-1}\sigma, \tag{6}$$

and the stress-dependent Young's modulus $E_e(\sigma)$ is written according to the empirical relationship

$$E_e(\sigma) = E_e^+ + (E_e^- - E_e^+)\exp(-D\sigma) \tag{7}$$

obtained as approximations that fit a number of experiments (see, e.g., Ref. 19 and references therein). The constants E_e^-, E_e^+, and D are selected via numerical trials, and their values are close to the those listed in Ref. 19. For completeness, we define the frozen state function by the approximation

$$\varepsilon_f^r(\sigma) = a\varepsilon_e^r(\sigma), \tag{8}$$

where the factor a is a constant lying within the interval $0<a<1$. For example, in the linear theory, a relationship such as Eq. (8) finds its justification in stating that the ratio of the equilibrium sound velocity to the frozen one is independent of stress. When the time dependence of loading $\sigma=\sigma(t)$ (i.e., the stress protocol) is known, Eq. (5) can be solved. As a rule, we use an initial condition in the form $\varepsilon^r(t=0)=\varepsilon_e^r(\sigma(t=0))$.

Figures 2 and 3 illustrate the relaxation mechanism. The stress protocols for Figs. 2 and 3 qualitatively correspond to

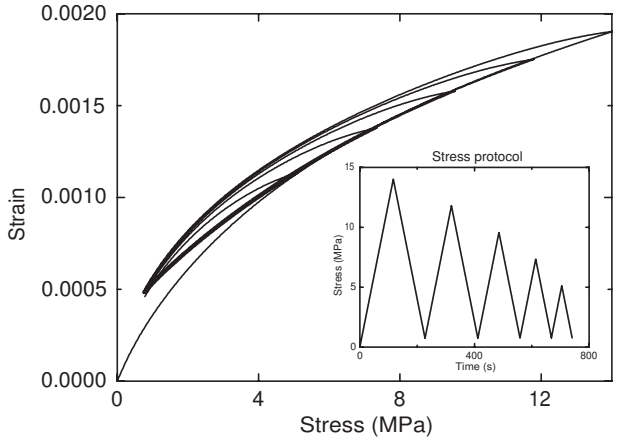

FIG. 2. Modeling the Boitnott experiment (Ref. 2) using only the standard solid relaxation mechanism.

the loading in works by Boitnott (see Fig. 1 in Ref. 7) and Hilbert *et al.* (see Fig. 2 in Ref. 7) accordingly. The constants in the state equations [Eqs. (5)–(8)] are taken to be the same for both pictures. The best correspondence with experiments was obtained for a relaxation time τ of 18 s; the other constants are $E_e^-=1.5$ GPa, $E_e^+=32$ GPa, $D=0.05$ MPa^{-1}, and $a=0.7$. Modeling Boitnott's experiments leads to almost ideal results. In contrast, Hilbert's experiment cannot be adequately described by the sole relaxation mechanism, inasmuch as it does not close the small loops through the stress-strain cusps for any assignment of constants in the state equations. Thus, the relaxation mechanism by itself does not explain end-point memory.

B. Sticky-spring mechanism

In order to develop a means to explain the end-point memory of the stress-strain curves mentioned above, it helps examining the stress-strain curves for Meule sandstone in the work by Darling *et al.*[4] For this purpose, we select only important parts of the data of Darling *et al.* and depict them

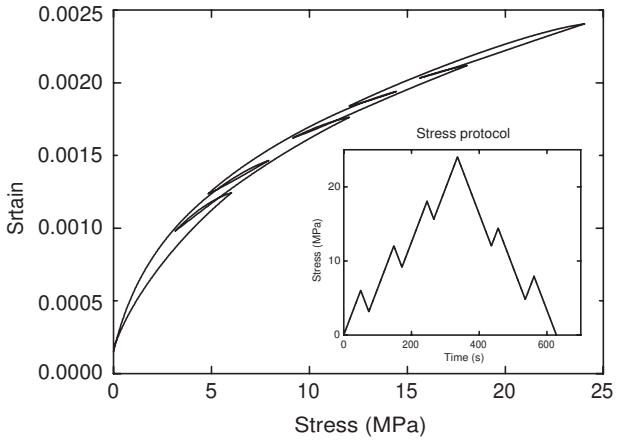

FIG. 3. Modeling the experiment of Hilbert *et al.* (Ref. 3) using only the standard solid relaxation mechanism. The theoretical curve for the unconditioned state is not shown here because its experimental counterpart is not available.

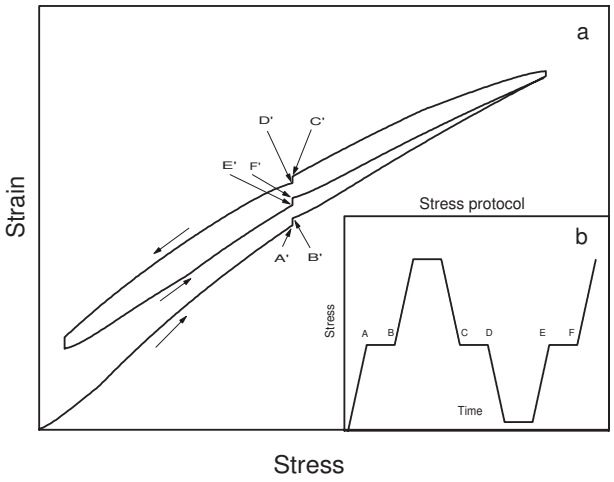

FIG. 4. Features of the stress-strain relations for Meule sandstone (Ref. 4) (qualitative picture).

qualitatively in Fig. 4. Points corresponding to each other in the stress protocol picture [Fig. 4(b)] and stress-strain picture [Fig. 4(a)] are marked by the same capital letters and are unprimed and primed, respectively. In the time intervals AB, CD, and EF, stress is constant. The fact that the points A', C', and E' do not coincide with the respective points B', D', and F' can be explained by relaxation alone. However, relaxation by itself should inevitably lead the experimentally distinct points D' and F' (and even B') to coincide. To resolve this problem and understand the discrepancy, it is necessary to include an additional mechanism. We call this additional process the sticky-spring mechanism and, for the sake of convenience, formulate it separately from the other mechanisms.

A prototype system to illustrate this mechanism is given in Fig. 5. The system consists of a closed cylinder containing a cork plug. The quantity of gas in the closed end is fixed, and its pressure p_i supplies the elastic restoring force. In addition, there is friction between cork and tube walls. We treat this friction as independent of cork velocity. Such friction arises in thermodynamical systems when the interior equilibration process is slow in comparison with the typical time of loading.[15]

In terms of the cork-tube device, the maximum frictional force is taken to be proportional to the threshold pressure p_t

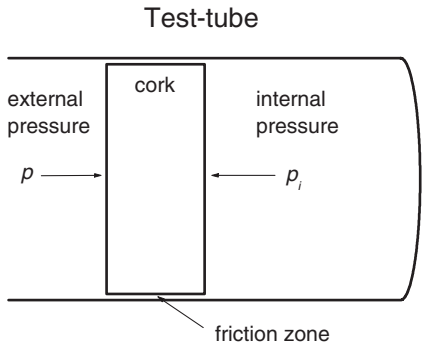

FIG. 5. Analog model to illustrate the sticky-spring mechanism.

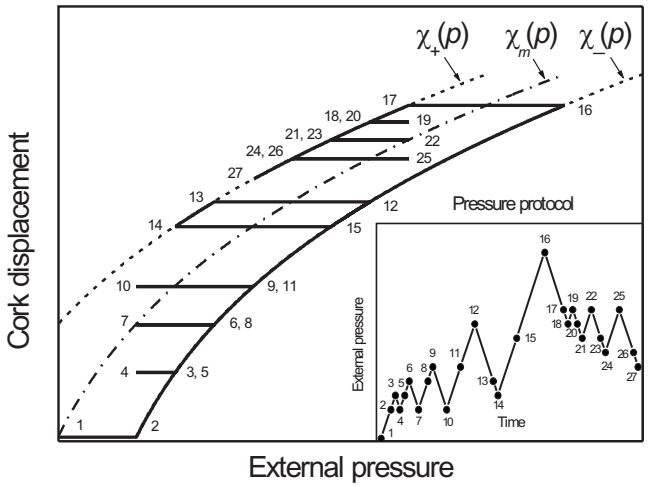

FIG. 6. Cork displacement in response to external pressure. The curve of marginal equilibrium $\chi=\chi_m(p)$ is marked by a dash-dotted line.

(a positive value) that must be overcome by external pressure p against an internal p_i (or vice versa) in order for the cork to be pushed from one position into another. If we assume the cork to be massless, its displacement χ along the tube as a function of time t obeys the following first-order differential equation:

$$\frac{d\chi}{dt} = \theta(\dot{p})\,\theta(\chi_-(p)-\chi)\frac{d\chi_-(p)}{dp}\dot{p} + \theta(-\dot{p})\,\theta(\chi-\chi_+(p)) \times \frac{d\chi_+(p)}{dp}\dot{p}, \tag{9}$$

in which the functions

$$\chi_-(p) \equiv \chi_m(p-p_t), \quad \chi_+(p) \equiv \chi_m(p+p_t) \tag{10}$$

are determined by

$$\chi_m(p) = l_0 - \frac{p_0 l_0}{p}. \tag{11}$$

Here, $\theta(z)$ is the Heaviside step function, $p_0 l_0$ is a constant characterizing the quantity of gas in a working volume of the cylinder, and l_0 is a length that fixes the working point of the cork-tube nonlinear device. Thus, $l_0-\chi$ is simply the running position of the cork with respect to the back of the tube.

Some aspects of the sticky-spring mechanism are presented in Fig. 6, which illustrates the dependence of cork displacement χ on external pressure p. For this purpose, Eq. (9) has been numerically integrated from the initial condition $\chi(t=0)=0$ using the pressure protocol given in Fig. 6(b). The essential feature of the stickyspring mechanism consists in producing a stripe-like continuum of stationary states between the curves $\chi=\chi_-(p)$ and $\chi=\chi_+(p)$ as in Fig. 6. Only in the limit of very small threshold pressure $p_t \to +0$ do these curves come together and give rise to a single curve $\chi=\chi_m(p)$. This medial curve turns out to bisect the stripe and can be thought as the equilibrium curve of the process in the limiting case of $p_t \to +0$. Another essential part of this mechanism is its elastic component manifested through the inclination of stripe $\chi_-(p)<\chi<\chi_+(p)$ with respect to the p axis.

Summarizing the principal features of the sticky-spring mechanism [Eqs. (9) and (10)] as applied to sandstones, we postulate the stress-strain relation to be

$$\frac{d\varepsilon^s}{dt} = \theta(\dot{\sigma})\,\theta(\varepsilon_-(\sigma)-\varepsilon^s)\frac{d\varepsilon_-}{d\sigma}\dot{\sigma} + \theta(-\dot{\sigma})\,\theta(\varepsilon^s-\varepsilon_+(\sigma))\frac{d\varepsilon_+}{d\sigma}\dot{\sigma}. \tag{12}$$

Here, the partial strain ε^s is associated with the sticky-spring contribution to the total strain ε, while the functions $\varepsilon_-(\sigma)$ and $\varepsilon_+(\sigma)$ are determined via the medial equilibrium state function $\varepsilon^s_m(\sigma)$ and two positive threshold stresses σ_+ and σ_- as follows:

$$\varepsilon_-(\sigma) \equiv \varepsilon^s_m(\sigma-\sigma_-), \quad \varepsilon_+(\sigma) \equiv \varepsilon^s_m(\sigma+\sigma_+). \tag{13}$$

We note that no restrictions are imposed on the threshold values σ_- and σ_+ that are responsible for the friction. In principle, they can be functions of stress σ.

For the function $\varepsilon^s_m(\sigma)$, we assume

$$\varepsilon^s_m(\sigma) = \varepsilon^r_e(\sigma). \tag{14}$$

In accord with thermodynamic principles, Eq. (14) thus requires that the final position of a truly equilibrium state be independent of the origin of the internal processes that led to this equilibrium.

Within the Preisach-Mayergoyz (PM) approach,[6] the qualitative distribution $\rho^s(P_c,P_o)$ for the sticky-spring mechanism can be written as

$$\rho^s(P_c,P_o) = A^s(P_c,P_o)[\theta(P_c-\sigma_+)\,\theta(\sigma_++\sigma_--P_c)\,\delta(P_o) + \theta(P_c-(\sigma_++\sigma_-))\,\delta(P_c-P_o-(\sigma_++\sigma_-))], \tag{15}$$

where notations are taken from Ref. 6.

Because the sticky-spring mechanism employs fewer adjustable parameters (constants) than do PM models, we use this mechanism to describe quasistatic loading in rocks. Furthermore, if we consider possible physical interpretations of the sticky-spring effects, it seems plausible that they capture the most essential features in opening-closing of sticky microcracks.

In Sec. IV, we show that, in the proper combination, the standard solid relaxation mechanism and the sticky-spring mechanism enable us to model relaxation steps on the conditioned curves under a fixed load (Fig. 4) and the effect of end-point memory, respectively. However, to include the unconditioned portion of the curves, we must invoke a mechanism that takes plastic deformation into account.

C. Permanent plastic deformation mechanism

We note that the permanent plastic deformation mechanism can, in principle, be treated within the relaxation mechanism, provided we include an additional set of relaxation parameters. However, because the permanent plastic deformation mechanism is responsible for the difference be-

TABLE I. Fitting parameters.

τ (s)	E_e^- (GPa)	E_e^+ (GPa)	D (MPa^{-1})	σ_- (MPa)	σ_+ (MPa)	E_p (GPa)	a	b
3	5	23	0.03	4	4	70	0.2	0.8

tween the unconditioned and conditioned states, we prefer to separately extract it as an appropriately adjusted relaxation mechanism.

Taking into account the intuitively understandable features of permanent plastic deformation, we postulate that under compression, i.e., during increasing initial loading $\dot{\sigma}>0$, the sample, on one hand, must contract with a permanent plastic contribution ε^p to total strain to obey a linear Hooke-like law $\varepsilon^p=\sigma/E_p$ (where the appropriate Young's modulus E_p is presumed to be stress independent). On the other hand, it must simultaneously experience interior irreversible deformations. Conversely, when external loading decreases, $\dot{\sigma}<0$, the plastic component ε^p must remain fixed. To formalize the statements above, the state equation for the permanent plastic deformation mechanism can be described as

$$\frac{d\varepsilon^p}{dt}=\frac{\theta(\dot{\sigma})\theta(\sigma/E_p-\varepsilon^p)\dot{\sigma}}{E_p}. \tag{16}$$

According to this mechanism, once a peak loading is achieved, the possible store of plastic deformation in the rock sample becomes saturated. Thereafter, when loading less than the peak stress, the permanent plastic deformation mechanism does not appear as subsequent cycles. Through the Heaviside function, only an unconditioned curve manifests permanent plastic deformation; on conditioned curves, it does not contribute.

Similar to the sticky-spring mechanism, the distribution in the PM space [see Fig. 2(a) in Ref. 6] for permanent plastic deformation mechanism can be obtained from

$$\rho^p(P_c,P_o)=A^p(P_c,P_o)\delta(P_o). \tag{17}$$

It is necessary to note that the sticky-spring mechanism and the permanent plastic deformation mechanism can be considered as independent of each other, as are individual elements in PM space.

The separation of the sticky-spring mechanism and the permanent plastic deformation mechanism can have a physical interpretation. In the experimental results,[2–4] each increment of stress (starting at zero stress) beyond the previous highest stress produces irreversible changes in the rock fabric as crack surfaces slide and asperities are crushed. The permanent plastic mechanism is a means of incorporating these irreversible changes. In a regime where stress cycles at stresses less than the maximum previously achieved, the sticky-spring mechanism is applied. It may be that the PM approach can cover the whole stress range, yet there is utility in the present approach where damaging stresses are separated from a regime in which stress cycles are associated with reversible changes in the rock.

It is interesting to observe that Belinskiy has experimentally revealed the pure permanent plastic deformation under collision of steel balls in chain with plumbum layers.[20]

IV. SIMULATION OF STRESS-STRAIN RELATIONS

In the previous section, we have suggested three mechanisms by which interior interaction processes in sandstones are assumed to take place. Because the physical origins of these processes have not been well established, we use a phenomenological approach in which they are not concretely defined. In computing the counterparts of the available experimental data, the processes modeled by both the standard solid relaxation and the sticky-spring mechanisms can be treated using only a minimal number of phenomenological parameters, i.e., the number adopted in Secs. III A and III B. However, when describing more precise experiments, the suggested models have the potential to be modified by extending the number of relaxation and sticky-spring processes.

Taking into account all three developed mechanisms (standard solid relaxation, sticky-spring, and permanent plastic deformation), we rely upon the minimum number of processes, i.e., only a single process for each mechanism. For loading by a given stress protocol, we can solve Eqs. (5), (12), and (16), with the initial conditions $\varepsilon^r(t=0)=\varepsilon^s(t=0)=\varepsilon^p(t=0)=0$ and find the total strain ε as a linear combination of partial strains:

$$\varepsilon=b(\varepsilon^r+\varepsilon^p)+(1-b)(\varepsilon^s+\varepsilon^p). \tag{18}$$

Here, the constant b is bounded inside the interval $0\leqslant b\leqslant 1$. Clearly, at $b=1$, we have the relaxation mechanism with permanent plastic deformation only, while at $b=0$, we retain only the sticky-spring mechanism plus permanent plastic deformation. Choosing relation (18) as a linear combination and keeping in mind definition (14), we are able to tune the single parameter b to obtain a physical condition such that the true equilibrium state is independent of any type of interior relaxation process.

If the stress is fixed at one moment, then the relaxation mechanism moves the whole system to some new equilibrium during a characteristic relaxation time. Owing to the sticky-spring mechanism plus the permanent plastic deformation mechanism, there can be several equilibrium states at the same stress. The ambiguity of equilibrium state dependence on stress can be found in Ref. 14.

The best fits of the calculated results as applied to all three groups of experiments on Berea sandstone[2–4] (see also Fig. 1) were obtained with the parameters listed in Table I. Note that these parameters are applied when we consider the combination of all three mechanisms, in contrast to the pa-

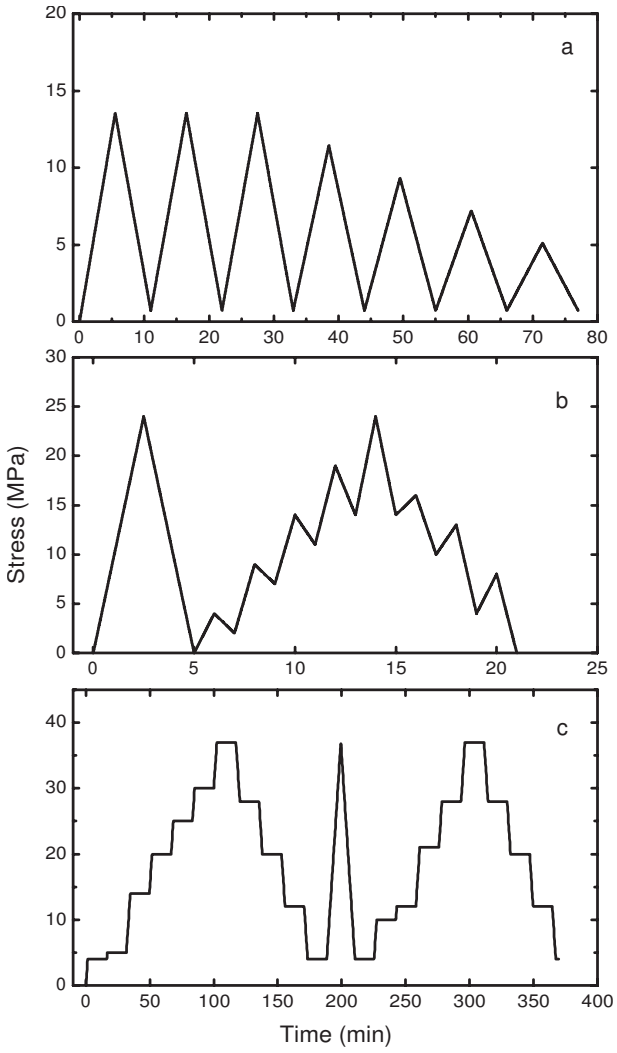

FIG. 7. Stress protocols for Fig. 8. The figures marked by letters *a*, *b*, and *c* correspond to the curves *a*, *b*, and *c* in Fig. 8, respectively.

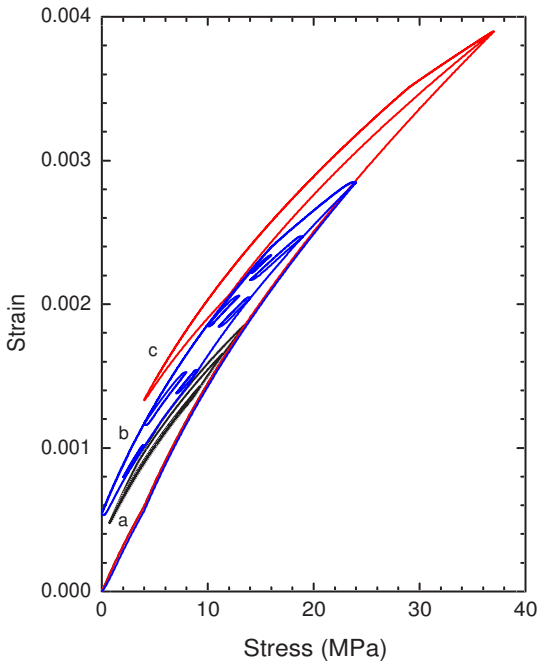

FIG. 8. (Color online) Computerized modeling of stress-strain trajectories for Berea sandstone. Curve *a* relates to the experiment of Boitnott (Ref. 2), curve *b* models the experiment of Hilbert *et al.* (Ref. 3), and curve *c* reproduces the experiment of Darling *et al.* (Ref. 4).

rameters applied in Sec. III A for Figs. 2 and 3 when only the relaxation mechanism was analyzed.

Results of the numerical simulation are presented in Figs. 7 and 8. Comparing the calculated curves (Fig. 8) with experimental data (Fig. 1), we observe an acceptable coincidence of these results both qualitatively and quantitatively. First, we find the small loops in curve *b* of Fig. 8 that models the experiment of Hilbert *et al.*[3] These loops are closed at the cusps. Unfortunately, in experimental curves for Berea sandstone, it is difficult to reveal the features that are present in Meule sandstone (Fig. 1 in Ref. 4), i.e., to precisely observe the steps caused by sample relaxation under fixed load, e.g., in Fig. 4. This difficulty could be explained by the exceptional smallness of typical relaxation times for Berea sandstone as compared with typical times in the experimental stress protocol. For this reason, Berea sandstone features related to relaxation under fixed load are simply not seen in our theoretical curve *c* of Fig. 8 that models the experiment of Darling *et al.*[4] However, the relaxation mechanism cannot be completely removed because it plays an important role in describing end-point memory as manifested by the small loops on the theoretical curve *b* in Fig. 8, which reproduces the experiment of Hilbert *et al.*[3] On one hand, it is precisely the effect of small but finite relaxation time that enables one to close a small loop through a cusp (curve *b* in Fig. 8 once again). On the other hand, the relaxation provides the means to produce the small loops in the modeling.

V. CONCLUSION

This paper suggests a phenomenological model to describe the stress-strain properties of Berea sandstone under quasistatic loading. Analysis of experimental observations has demonstrated the need to invoke several mechanisms that are responsible for interior equilibration processes in sandstone: the standard solid relaxation mechanism, the sticky-spring mechanism, and the permanent plastic deformation mechanism. To justify these mechanisms, we have used an approach in which the interior processes in a sample are not explicitly defined, which drastically simplifies the mathematical description. Only by properly combining all three mechanisms are we able to obtain acceptable models. Moreover, it was shown that the first two (the relaxation and sticky-spring mechanisms) can each be restricted to one process for each mechanism. The resulting treatment reproduces extremely complex stress-strain trajectories with only nine adjustable parameters. However, if it is required to describe other, more precise experiments, then the model can be properly modified because it is possible to invoke a number of relaxation times for the standard solid relaxation mechanism

and friction parameters for the sticky-spring mechanism. As for the permanent plastic deformation mechanism, we presently do not know how it could be generalized to include more than one phenomenological parameter.

Because of the proposed treatment of quasistatic stress-strain relations, it becomes possible to produce an adequate and self-consistent simulation that both qualitatively and quantitatively describes the principal features of experimental data by Boitnott,[2] Hilbert *et al.*,[3] and Darling *et al.*[4] for Berea sandstone. The model correctly reproduces both the large loops and, equally importantly, the small loops in stress-strain trajectories (end-point memory effect).

ACKNOWLEDGMENTS

J.A.T. and T.J.S. thank the Geosciences Research Program, Office of Basic Energy Sciences of the U.S. Department of Energy for sustained assistance. V.O.V. is grateful to V. A. Danylenko for stimulating criticism and helpful discussions.

*Author to whom correspondence should be addressed; vakhnenko@ukr.net
†vakhnenko@bitp.kiev.ua
‡tencate@lanl.gov
§shanklan@lanl.gov

[1] F. D. Adams and E. G. Coker, *An Investigation Into the Elastic Constants of Rocks, More Especially With Reference to Cubic Compressibility* (Carnegie Institute of Washington, Washington, DC, 1906).
[2] G. N. Boitnott, Proceedings of the Numerical Modeling for Underground Nuclear Test Monitoring Symposium, Los Alamos National Laboratory Report No. LA-UR-93-3839, 1993 (unpublished), p. 121. Report available upon request from the Los Alamos National Laboratory library.
[3] L. B. Hilbert, Jr., T. K. Hwong, N. G. W. Cook, K. T. Nihei, and L. R. Myer, in *Rock Mechanics: Models and Measurements, Challenges, from Industry*, edited by P. P. Nelson and S. E. Laubach (Balkema, Rotterdam, 1994), p. 497.
[4] T. W. Darling, J. A. TenCate, D. W. Brown, B. Clausen, and S. C. Vogel, Geophys. Res. Lett. **31**, L16604 (2004).
[5] K. T. Nihei, L. B. Hilbert, Jr., N. G. W. Cook, S. Nakagawa, and L. R. Myer, Int. J. Rock Mech. Min. Sci. Geomech. Abstr. **37**, 121 (2000).
[6] K. R. McCall and R. A. Guyer, J. Geophys. Res. **99**, 23887 (1994).
[7] R. A. Guyer, K. R. McCall, G. N. Boitnott, L. B. Hilbert, Jr., and T. J. Plona, J. Geophys. Res. **102**, 5281 (1997).
[8] B. I. Pandit and J. C. Savage, J. Geophys. Res. **78**, 6097 (1973).
[9] R. A. Guyer and P. A. Johnson, J. Mater. Process. Manuf. Sci. **9**, 14 (2000).
[10] J. A. TenCate, E. Smith, and R. A. Guyer, Phys. Rev. Lett. **85**, 1020 (2000).
[11] O. O. Vakhnenko, V. O. Vakhnenko, T. J. Shankland, and J. A. TenCate, Phys. Rev. E **70**, 015602(R) (2004).
[12] O. O. Vakhnenko, V. O. Vakhnenko, and T. J. Shankland, Phys. Rev. B **71**, 174103 (2005).
[13] M. Bentahar, H. El Aqra, R. El Guerjouma, M. Griffa, and M. Scalerandi, Phys. Rev. B **73**, 014116 (2006).
[14] V. E. Gusev, W. Lauriks, and J. Thoen, J. Acoust. Soc. Am. **103**, 3216 (1998).
[15] V. O. Vakhnenko, J. Math. Phys. **40**, 2011 (1999).
[16] C. Zener, *Elasticity and Anelasticity of Metals* (The University of Chicago Press, Chicago, 1948).
[17] L. I. Mandelshtam and M. A. Leontovich, Zh. Eksp. Teor. Fiz. **7**, 438 (1937).
[18] L. D. Landau and E. M. Lifshitz, *Fluids Mechanics* (Pergamon, New York, 1988).
[19] A. Kaselow and S. A. Shapiro, J. Geophys. Eng. **1**, 1 (2004).
[20] I. V. Belinskiy, V. A. Lemeshko, and V. V. Grzhybovskiy, Rep. NAS Ukraine (to be published).